CHAPTER II
THEORETICAL BACKGROUND AND LITERATURE REVIEW

2.1 Corrosion of Steel

Corrosion is the destruction or deterioration of materials because of reaction with its environment. Severe corrosions may occur if the environment is high temperature or high pressure. Severe corrosions can lead to costly outages and repairs and can affect plant reliability and safety. In some cases, however, corrosion is beneficial or desirable. For example, chemical machining or chemical milling, unmarked areas are exposed to acid and excess metal is dissolved. Another beneficial corrosion process is to obtain better and more uniform appearance in addition to a protective corrosion product on the surface in anodizing of aluminum (Fontana 1988).

2.1.1 Flow Accelerated Corrosion (FAC)

Flow accelerated corrosion (FAC), also known as flow assisted corrosion, is the chemical dissolution of surface oxide and base metal, accelerated by flow and flow impingement. This process involves a magnetic oxide film formation on the carbon steel surface. The oxide film acts as a protective oxide layer due to the reaction between dissolved oxygen in flowing water or water/steam systems and the carbon steel surface. The protective oxide layer on the metal surface dissolves from the surface as dissolved iron, or forms a solid corrosion product which can be mechanically swept from the metal surface and carried downstream. A new oxide layer forms on exposed patches at the bare metal with continual removed and reformed oxide, and thus the metal loss continues resulting in wall thinning as shown in Figure 2.1.

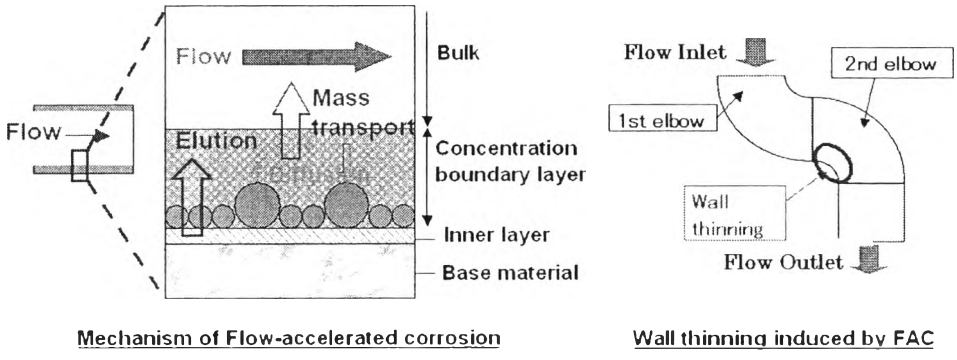

Figure 2.1 Mechanism of flow accelerated corrosion and wall thinning induced by FAC (http://afre.qse.tohoku.ac.jp/research/FAC/e-index.html).

FAC can be anticipated whenever a susceptible metal is exposed to specific environmental conditions. The more important variable for FAC are temperature, pH, fluid velocity and dissolved oxygen concentration.

2.2 Mechanism of Oxide Growth and Hydrogen Evolution in Corrosion

In CANDU reactors, the observed iron oxide on the metal is magnetite (Fe_3O_4). This type of oxide film behaves like a corrosion resistance film to the steel from the corrosive environment. The morphology of the oxide film is influenced by the chemical composition of the alloy, exposure conditions and surface finishing (Lister, Arbeau et al. 1994).

Carbon steel corrodes in high temperature water and forms a double layer in supersaturated conditions, known as the Potter and Mann layer. The inner layer consists of small magnetite crystals that grow into the metal, replacing the corroded volume (Potter and Mann 1962). This layer grows at the metal-oxide interface and is compact and adherent (Potter and Mann 1963) since it nucleates in the confined space. The outer layer consists of larger magnetite crystals since it grows by outward diffusion of the metal ions, especially iron, along oxide grain boundaries without volume constraint. The schematic of double oxide layers formed on carbon steel is shown in Figure 2.2.

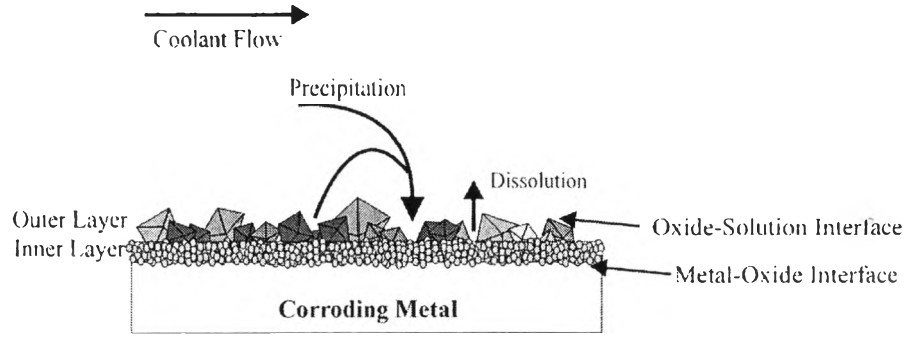

Figure 2.2 Schematic of the double oxide layer formed on carbon steel (Lister, Slade et al. 1997).

The corrosion of carbon steels and low alloy steels in high temperature water, in the absence of oxygen, involves the transport of oxygen-bearing species to the metal/oxide interface and outward movement of metal ions to the solution. When the solution becomes saturated with soluble iron, an outer magnetite layer is nucleated and grows on the surface. The net result is a double magnetite layer.

In the absence of oxygen, the inward movement of oxygen-bearing species occurs by diffusion either water molecules, oxygen ions or hydroxide ions. Since oxygen ions involve the formation of oxide films only after a sufficiently anodic potential is imposed and a de-protonation of water takes place, resulting in the loss of protons to the solution and oxygen ions migrating toward the steel surface. Oxygen ions, therefore, cannot be the diffusion species. Since the oxide films are thin, the electric charge strength across the film is high. The established electric field will block the negative charged ions, such as OH^- from moving towards the steel surface. This eliminates hydroxide ions as the diffusion species. Therefore, the oxygen-baring species involving the formation of the magnetite layer is probably water (Cheng and Steward 2004).

A proposed schematic of the magnetite film formed on a steel surface in a high temperature water solution is shown in Figure 2.3; water molecules diffuse through the inner oxide layer and react directly with steel at the steel/oxide interface. Iron dissolution occurs where an oxide layer exists. Protons at the oxide/water interface diffuse through the oxide layer to consume the electrons produced by anodic

reactions and discharge as hydrogen atoms at the steel/oxide interface. The relevant reactions occurring at the steel/oxide interface are:

$$3Fe + 4H_2O \rightarrow Fe_3O_4 + 8H^+ + 8e^- \quad (2.1)$$

$$Fe \rightarrow Fe^{2+} + 2e^- \quad (2.2)$$

$$H^+ + e^- \rightarrow H \quad (2.3)$$

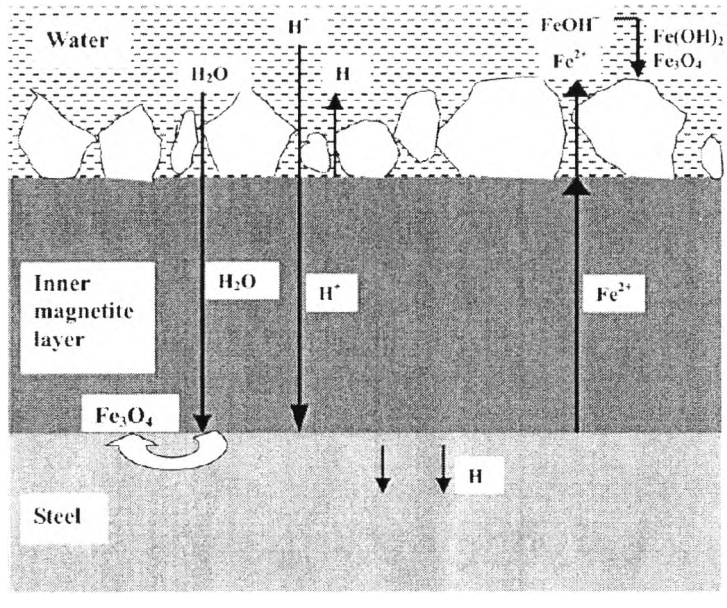

Figure 2.3 Schematic view of the formation of the magnetite film on the steel surface in high temperature water (Cheng and Steward 2004).

The ferrous ions diffusing out of the oxide layer exist as $Fe(OH)^+$ in high temperature water must stabilize themselves by decreasing their charge/radius ratios through hydrolysis to form hydrous iron ions. The hydrous iron ions will deposit as loose $Fe(OH)_2$ once the saturation of the iron ion is achieved. The outer deposition of the magnetite layer is then formed in high temperature water, accompanying the discharge of hydrogen ions. Therefore, the electrochemical reactions occurring at the oxide/water interface are:

$$3Fe(OH)^+ + H_2O \rightarrow Fe_3O_4 + 5H^+ + 2e^- \quad (2.4)$$

$$2H^+ + 2e^- \rightarrow H_2 \quad (2.5)$$

The reaction above indicates that hydrogen gas is produced by the steel corrosion process.

Study of hydrogen emission during steel corrosion (Tomlinson 1981; Tomlinson and Cory 1989) showed that produced protons from the corrosion process diffuse in both directions across the oxide, with the direction and magnitude of the proton flux being dependent on the structure of oxide layer. Hydrogen atoms are formed at both the metal/oxide interface and the oxide/water interface, hydrogen atoms are either discharged at the oxide/water interface by electron diffusion across the oxide or diffusion through the oxide as protons which are discharged at the metal/oxide interface. Under the concentration and potential gradient, protons at the oxide/water interface diffuse rapidly through the oxide layer and discharge as hydrogen atoms at the metal/oxide interface.

The experimental evidence from the above study indicates that up to 90% of the hydrogen atoms are generated at the metal/oxide interface during the corrosion of steels by high temperature deaerated water. More than 99% of these hydrogen atoms will diffuse through the steel at the temperature of interest since it is generally accepted that the hydrogen diffusivity in an oxide film is very low. Hydrogen diffuses through the metal 330 times faster than through the oxide (Tomlinson 1981). He also suggested that if the rate of growth of the inner layer per rate of growth of the outer layer is constant, then the ratio of hydrogen emission from metal and oxide surfaces should also be constant. Furthermore, the fraction of hydrogen passing through the steel appears to increase with the amount of oxide deposited on the tube surface.

2.3 Hydrogen Probe for Monitoring Corrosion

2.3.1 Hydrogen Probe Principle

The concept of the hydrogen effusion probe is based on the fact that one of the cathodic reaction products in the corrosion process is hydrogen. The hydrogen atoms thus generated diffuse through the pipe and are liberated at the exterior surface. Therefore the hydrogen probe can measure the corrosion rate by measuring hydrogen release at the surface. One advantage of exterior hydrogen monitoring is

that it does not require penetration of the pipe wall in order to obtain the corrosion rate since the hydrogen probe is installed on the outside pipe wall.

Not entirely the case, for calculation the quantification of this method assumes that all of the hydrogen liberated in the corrosion reaction diffuses through the steel vessel wall instead of being liberated as hydrogen gas at the inside surface. This method is in practice limited to steel, which has a high hydrogen diffusivity and low solubility of hydrogen (Davis, Destefani et al. 1987).

The feeder thinning occurs because iron atoms (Fe^{2+}) in the steel dissolve into the coolant as a consequence of FAC. The hydrogen probe can measure the pipe thinning rate since the quantity of hydrogen effusing through the carbon steel pipe is proportional to the rate that iron is lost into solution. It is assumed that one mole of hydrogen gas is produced from one mole of iron ion loss. The reaction for this relation is shown below.

$$Fe + 2H^{+} \rightarrow Fe^{2+} + 2H \qquad (2.6)$$

The hydrogen probe system operates under vacuum. In principal, hydrogen effusing from the pipe is collected in the chamber outside of the pipe wall and causes the pressure to rise. The pressure transducer or pressure gauge measures the hydrogen pressure increase which can be used to calculate wall thinning rates.

An important feature of the hydrogen flux probe monitoring is that it is a real-time device, which can detect short-term upsets in the process. By getting real-time data from corrosion monitoring, operators can relate this data to events that cause the corrosion. This allows them to lower corrosion rates by adjusting or eliminating corrosion-causing events.

The rate of corrosion is related to hydrogen evolution based on Equation 2.6. One mole of H_2 is produced for one mole of Fe^{2+} loss.

$$C = \frac{a\dfrac{\partial n}{\partial t}M}{A\rho}, \qquad (2.7)$$

where C is corrosion rate (cm/yr),

M_{Fe} is molar mass of iron which is 55.85 g/mol,

A is internal area of pipe (cm^2),

ρ_{Fe} is the density of iron which is 7.86 g/cm^3

a is the conversion of days to year (365 days/yr), and

$\frac{\partial n}{\partial t}$ is a daily accumulation of hydrogen molecules in a unit of moles/day.

Since hydrogen behaves as an ideal gas at low pressures, the number of moles of hydrogen accumulation per day can be related to the change in pressure by the ideal gas law.

$$\frac{\partial n}{\partial t} = \frac{\partial P}{\partial t}\frac{V}{RT_{eff}}, \qquad (2.8)$$

where $\frac{\partial P}{\partial T}$ is the rate of pressure increase in Pa/day,

V is total volume of the HEP which depends on an assembly of the HEP,

R is gas constant (8.314 $m^3 \cdot Pa/mol/K$), and

T_{eff} is the effective temperature (K) in the system.

Since various parts of the HEP system are exposed to different temperatures, the effective temperature therefore is the sum of the individual temperatures multiply by their respective volume percentage of the HEP system.

2.3.2 Hydrogen Effusion Probe (HEP)

The HEP consists of silver cup connected via silver and stainless steel tubing to a valve, pressure transducer, vacuum pump, and data acquisition system. In order to avoid the leaking of hydrogen from the device, high purity silver is used due to the low permeation rate of hydrogen through this metal at high temperature. The system temperature is measured by installed thermocouples. The main components of the HEP instrumentation unit are an isolation valve, a precision absolute pressure transducer, and a data acquisition and control system. The pressure transducer has a controlled internal temperature of 45°C and a limiting ambient operating temperature

of 40°C. Changes in ambient temperature affect the transducer reading. The data acquisition and control system is used to control the pump and valve operation, and also record readings from the transducer and thermocouples. The thermocouples provide temperature information to enable analysis of the data.

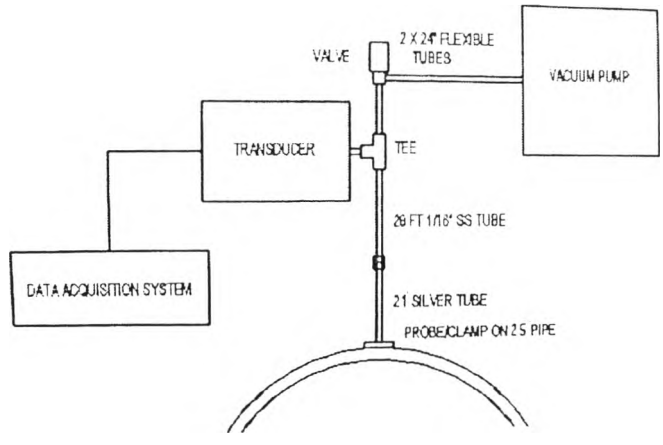

Figure 2.4 Schematic of HEP assembly (McKeen, Lalonde et al. 2007).

After a predetermined pressure is reached, 2000 Pa is recommended as the pressure range that is independent of hydrogen pressure, the data acquisition and control system would automatically repeat the test cycle. The vacuum pump switches on to evacuate the measuring volume and restart the cycle (McKeen, Lalonde et al. 2007).

Since 2001, Atomic Energy of Canada Limited (AECL) has performed a series of loop experiments funded by the CANDU® Owners Group Inc. (COG). The objective of this experiment is to study the FAC process that causes feeder wall thinning in the primary heat transport system of CANDU reactors. The results demonstrate that the rate of the FAC process in the tube can be examined online by measuring the rate of hydrogen that is produced from the FAC process, which effuses through the pipe wall. Consequently, this information led to the development of a Hydrogen Effusion Probe for monitoring of FAC.

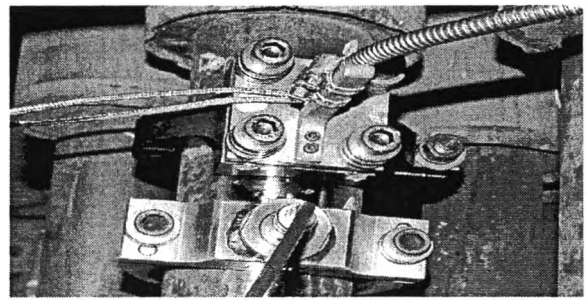

Figure 2.5 The HEP (top) and FOLTM (bottom) installed on feeder pipe at PLGS (McKeen, Lalonde et al. 2007).

In 2006, the Centre for Nuclear Energy Research (CNER) has been conducting HEP experiments. The objective of this project was to design and build an HEP that could be installed on an outlet feeder pipe at the Point Lepreau Generating Station (PLGS) and water wall tubing at the Coleson Cove Generating Station (CC). Figure 2.5 shows the HEP installed on a feeder pipe at the PLGS. Leak tests of the HEP were performed prior to start-up, and leak rates of 5 Pa/day which represents only a 0.25% contribution were determined. Data from the PLGS indicate that the HEP can provide an on-line indirect measurement of the feeder wall thinning rate which is approximately 60 μm per year. This feeder wall thinning rate can be compared with the rate measured by the FOLTM, which was installed next to the HEP for the same period of time. The data indicated that the feeder wall thinning rate from both devices was in agreement.

Although the accuracy of this rate has not yet been quantified, the feeder wall thinning rate is consistent with the expected rate for a straight length of outlet feeder pipe. The data from this experiment also suggest that the HEP is able to detect small changes in the FAC rate over short periods of time. The ability to monitor not only the corrosion of carbon steel outlet feeder pipe but also changes to the reducing/oxidizing (redox) chemistry may be possible.

2.4 Fundamental Law of Diffusion for Hydrogen

2.4.1 Sievert's Law

Hydrogen permeation through membranes has been modeled using the solution-diffusion approach, in which the hydrogen molecules dissociatively absorb on the metal surface, adsorb into and diffuse through the bulk in atomic H form, and recombine and desorb as molecular hydrogen at the permeate side. When diffusion of hydrogen atoms through the bulk metal is the rate limiting step and there are no surface effects on both sides of the specimen, hydrogen permeation flux is at steady state, J (mol/m^{2}s), and can be described by Sievert's law:

$$J = \frac{Q}{l}\left(\sqrt{P_{H_{2,f}}} - \sqrt{P_{H_{2,p}}}\right), \qquad (2.9)$$

where Q is the permeability of hydrogen through the membrane (mol/m.s.Pa$^{0.5}$),
L is the membrane thickness (m), and
$P_{H_{2,f}}$ and $P_{H_{2,p}}$ are the feed and permeate side of hydrogen partial pressure respectively.

The derivation of Sievert's law also assumes that the surface coverage of hydrogen at both the feed and permeate sides of the membrane is in equilibrium with the respective fluid phases, and that the adsorption equilibrium constant is the same on both sides:

$$C = KP_{H_2}^{0.5}, \qquad (2.10)$$

where C is the permeability atomic hydrogen concentration on the membrane surface,
K is the dissociative adsorption equilibrium constant and
P_{H_2} is the hydrogen partial pressure.

The 0.5 exponent comes from dissociative adsorption of a diatomic molecule and gives the square root of hydrogen pressure in the flux equation above.

Numerous measurements of Sievert and others prove that the solubility of gases having diatomic molecules is proportional to the square of the hydrogen gas pressure. According to Henry's law, if the molecular condition of the hydrogen gas in the metal is the gaseous state the solubility should be proportional to the hydrogen pressure, which may be expressed by the equation

$$P_{H_2} = kC_{H_2} \tag{2.11}$$

where P_{H_2} is the hydrogen partial pressure.

C_{H_2} is the concentration of molecular hydrogen in the metal.

On the other hand if the hydrogen gas in solution can be assumed to be dissociated, the equilibrium between atomic and molecular hydrogen in the metal is then expressed by the equation:

$$C_{H_2} = k_1(C_H)^2 \tag{2.12}$$

and from equation (2.11)

$$P_{H_2} = kC_{H_2} = kk_1(C_H)^2 \tag{2.13}$$

or

$$C_H = k_2\sqrt{P_{H_2}} \tag{2.14}$$

The solubility would, therefore, be proportional to the square root of the pressure. Since the rate of diffusion will depend on the concentration of gas in the metal it may be expected that diffusion will be proportional to the square root of the gas pressure which is in agreement with the experimental results as shown in Figure 2.6 for hydrogen/iron system.

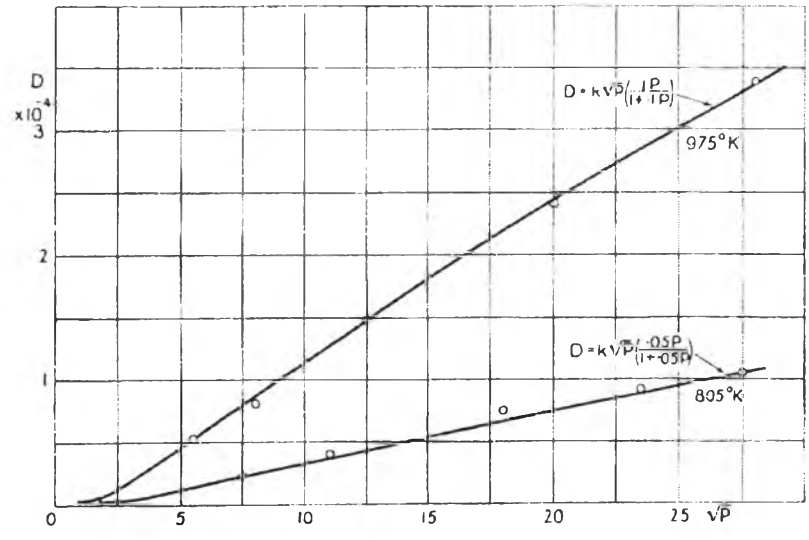

Diffusion of hydrogen through iron (Borelius and Lindblom)

Figure 2.6 Diffusion of hydrogen through iron; Borelius and Lindblom (Smithells and Ransley 1935).

Sievert's law is widely applied in analyzing hydrogen permeation through membranes, even in some cases where the assumptions made in deriving Sievert's law are not valid.

2.4.2 Mechanism of Hydrogen Transport Through Metals

Hydrogen permeation in metals and alloys is a complicated phenomenon. It is often assumed that the surface processes play an insignificant role in the gas permeation through metals and alloys since it is considered that they are much faster than the diffusion itself (Addach, Berçot et al. 2005).

In addition to its diffusion through the bulk metal, the permeation of hydrogen through steels involves its entrance at one surface and its exit at the other surface of the specimen. There are seven steps that take place before the hydrogen is detected on the output side of the specimen. Figure 2.7 shows the seven steps that take place in the permeation of a hydrogen isotope through a metallic membrane.

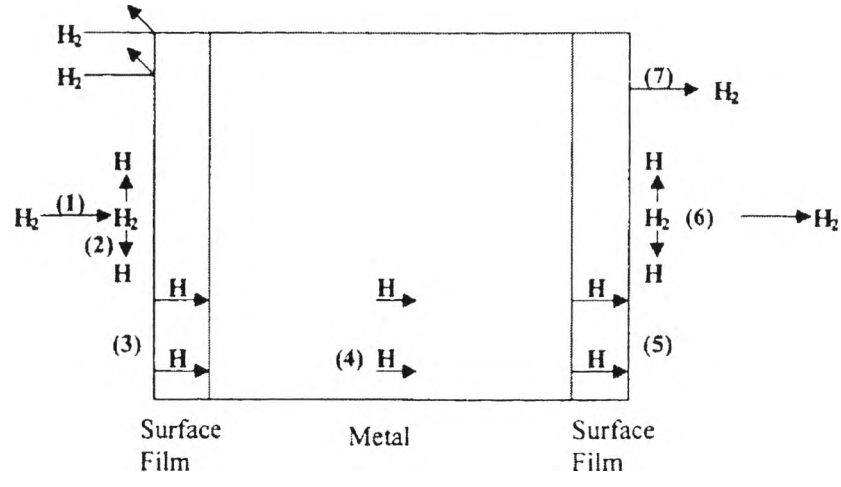

Figure 2.7 Seven steps of hydrogen permeation (Stone 1981).

This model takes into account the presence of surface films on both the input and output side of the specimen. The seven steps are:

1. Adsorption of hydrogen molecule on the surface.
2. Dissociation of the adsorbed molecule on the surface.
3. Permeation of dissociated atoms through the surface film (oxide).
4. Permeation of atoms through the metal.
5. Permeation of atoms through the film on the output side.
6. Reassociation of atoms to form H_2 molecule.
7. Desorption of the reassociated H_2 molecule.

If hydrogen is presented to the metal surface by electrochemical deposition or by means of a partially dissociated and/or ionized hydrogen gas, the dissociation step is avoided. Therefore in the case of corrosion, hydrogen is produced as hydrogen atoms which directly absorb and diffuse through the steel.

In the case of corrosion in CANDU reactors, hydrogen is produced as hydrogen atoms as a consequence of flow accelerated corrosion (FAC). Therefore hydrogen is present at the metal surface as atomic hydrogen which directly adsorbs and diffuses through the metal, the dissociation step is skipped.

2.4.3 Hydrogen Diffusivity in Oxide Films

Results from studies of the permeation of hydrogen through passivating films (Pyun and Oriani 1989) indicated that hydrogen transport through the passivated specimens is significantly retarded by the oxide films in the case of iron. Many years later, P. Bruzzoni (Bruzzoni, Carranza et al. 1999; Bruzzoni, Carranza et al. 1999) indicated that a diffusion coefficient of hydrogen in an oxide layer is very small or several orders of magnitude lower than iron. Therefore most of the hydrogen that is produced at the metal/oxide interface by FAC effuses through the metal, not through the oxide film.

Thin oxide films are shown to be excellent barriers against hydrogen diffusion. The diffusion coefficients of the oxide films are in range of $1.8\text{-}66\times10^{-17}$ cm^2/s while the diffusion coefficient of steel is about 10^{-8} cm^2/s. The value of the diffusion coefficient for the oxide depends on its chemical composition, and thickness due to changes in chemical composition of the oxide with thickness. Substrate and oxide grain size had no effect on diffusion rate (Piggott and Siarkowski 1972).

For studying the hydrogen permeation through metallic samples, a necessary requirement is that the hydrogen permeation rate be controlled by diffusion in the material of the specimen not by surface reaction. Oxide films, usually present on a metal surface, lower the degree of hydrogen dissociation and the permeation flux. This effect has been attributed to surface phenomena. Significant reductions in the hydrogen permeation rate are achieved even with very thin films. The removal of the surface layers that retard the hydrogen passage from the specimen is a necessary condition for hydrogen diffusivity measurement in metals.

SCHOMBERG and GRABKE (1996) studied the hydrogen permeation in the passive film on iron formed by chemical polishing. The results indicated that the film is nearly impermeable for hydrogen, even if the hydrogen is in the atomic or protonic state. They suggested that if the oxide films were situated on the hydrogen entry side, the surface reaction or hydrogen dissociation would be strongly retarded and hydrogen uptake would not be possible. On the other hand, hydrogen uptake and permeation of the oxide film may be possible if the hydrogen arriving at the iron/oxide interface is in an atomic/protonic state.

The study of hydrogen diffusion through steel without oxide film (Leelasangsai 2009) found that the hydrogen pressure after the removal of oxide film dropped rapidly. Leelasangsai (2009) suggested that the hydrogen diffusion through steel pipe is reduced by oxide film formed on both outside and inside surfaces. The oxide film acts as a significant barrier to hydrogen transport.

2.5 Iron Oxides

Iron oxides are a common compound which are widespread in nature and also can be synthesize in the laboratory. There are 16 types of iron oxides, these are consisting of oxide, hydroxide and oxide-hydroxide as show in the Table 2.1.

Table 2.1 The iron oxides (Cornell and Schwertmann 2003)

Oxide-hydroxides and hydroxides	***Oxides***
Goethite α-$FeOOH$	Hematite α-Fe_2O_3
Lepidocrocite γ-$FeOOH$	Magnetite Fe_3O_4 $(Fe^{II}Fe^{III}_2O_4)$
Akaganéite β-$FeOOH$	Maghemite γ-Fe_2O_3
Schwertmannite $Fe_{16}O_{16}(OH)_y(SO_4)_z \cdot nH_2O$	β-Fe_2O_3
δ-FeOOH	ε-Fe_2O_3
Feroxyhyte δ'-$FeOOH$	Wüstite FeO
High pressure $FeOOH$	
Ferrihydrite $Fe_5HO_8 \cdot 4H_2O$	
Bernalite $Fe(OH)_3$	
$Fe(OH)_2$	
Green Rusts $Fe^{III}_x Fe^{II}_y(OH)_{3x+2y-z}(A^-)_z$; $A^- = Cl^-$, $\frac{1}{2} SO_4^{2-}$	

The oxides are composed of iron (Fe) together with oxygen (O). Iron oxides are usually found in the trivalent state (contain Fe(II)); these oxides which are FeO, $Fe(OH)_2$ and Fe_3O_4 ($FeO \cdot Fe_2O_3$). Normally iron oxides consist of close packed arrays of anion (usually as a hexagonal (hcp) or cubic close packing (ccp). In which the interstitial is partly filled with divalent or trivalent Fe. Some types of oxide are described below:

Hematite (α-Fe_2O_3): Hematite is the oldest known Fe oxide mineral; it is widespread in rocks and soils. The color of this oxide is blood-red (Haima = blood in Greek). Hematite has the corundum (α-Al_2O_3) structure which is based on hcp anion packing. Hematite is extremely stable and often the end member of transformations of other iron oxides.

The commonest habits for hematite crystals are rhombohedral, platy and rounded. The plates vary in thickness and can be round, hexagonal or of irregular shape. These habits depend on hydrothermal conditions. The crystal structure of hematite has a less direction effect on crystal habit than goethite and for this reason; the habit of hematite is readily modified. In most cases of synthesized hematite crystals, the crystal faces that enclose the crystals have not been identified.

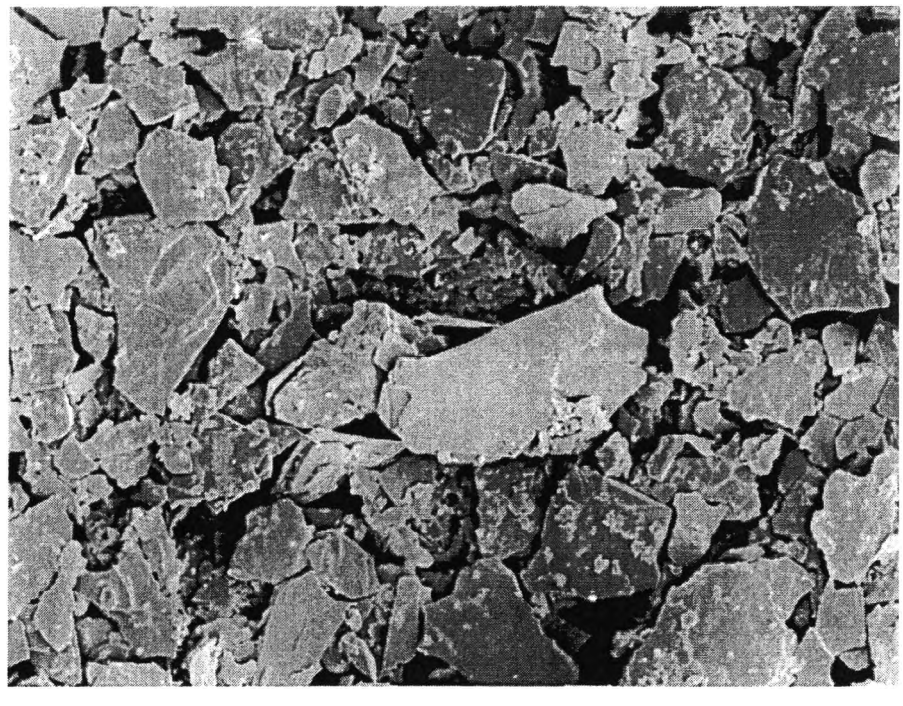

Figure 2.8 Micaceous hematite from Western Austraalia (Courtesy R. Giovanoli, referenced in The Iron Oxides: Structure, Properties, Reactions, Occurences and Ues).

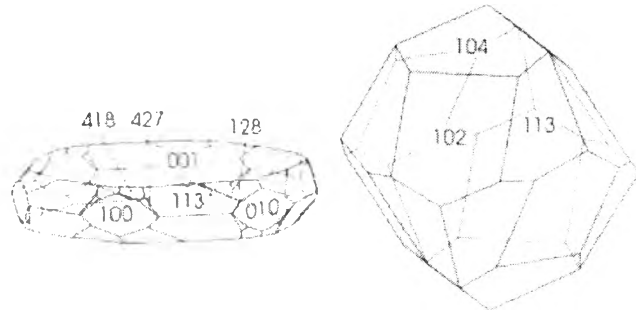

Figure 2.9 Crystal forms of platy and rhombohedral hematite (Courtesy H. Stanjek, referenced in The Iron Oxides: Structure, Properties, Reactions, Occurences and Ues).

Magnetite (Fe_3O_4): Magnetite is a black, ferrimagnetic mineral containing both Fe(II) and Fe(III). The structure of this type of oxide is an inverse spinel. Magnetite and titanomagnetite are responsible of magnetic properties of rocks. Magnetite occurs commonly as octahedral crystals bounded by {111} planes and as rhombododecahedra. Twinning occurs on the {111} plane and cubic terrace with their edge parallel to [110] was found on (100) face. The terraces are oriented along the main crystallographic direction. These structures can be examined by SEM technique.

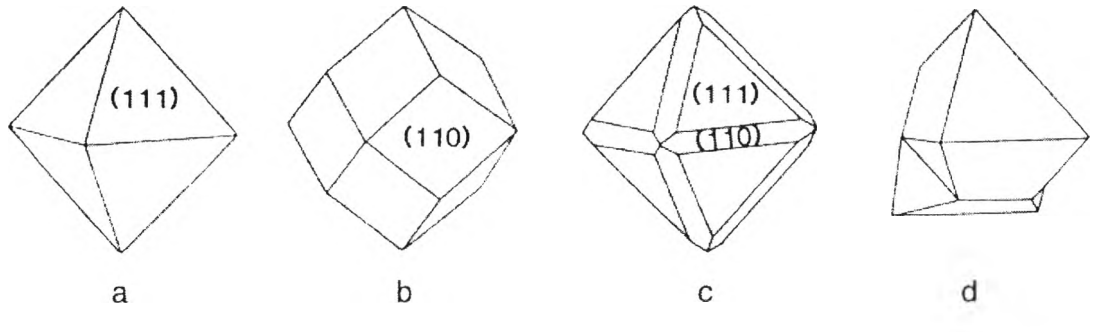

Figure 2.10 Crystal forms of magnetite a), c) octahedron; b) rhombodecahedron; d) twin.(Kostov, 1968, referenced in The Iron Oxides: Structure, Properties, Reactions, Occurences and Uses).

Maghemite (γ-Fe_2O_3): Maghemite is a red-brown, ferrimagnetic mineral isostructural with magnetite, but with cation deficient sites. It occurs as a weathering or heating product of other Fe oxides. Maghemite is usually formed by solid state transformation from another iron oxide or iron compound and almost always adopts the habit of its precursor; therefore, morphology of maghemite will depend on the starting material. Maghemite formed by oxidation of magnetite can be either cubic or irregular maghemite particles depending on the morphology of the parent material.

Wüstite (FeO): Wüstite is a black-color iron oxide which contains only di-valent Fe. It is usually non-stoichiometric (O-deficient). It has similar structure as NaCl and based on ccp anion packing. It is also an important intermediate in the reduction of iron ores. Wüstite is thermodynamically unstable below 570°C (Gaskell 1981), below this temperature, Wüstite is decomposed in to a mixture of Fe and Fe_3O_4 (Lecourt 1996). The basic morphology of wüstite is cubic; however, this compound is frequently obtained as very irregular particles. It is formed as irregular rounded crystals 20-100 μm across by reduction of hematite with H_2/H_2O at 800°C (Moukassi *et al.*, 1984 referenced in The Iron Oxides: Structure, Properties, Reactions, Occurences and Uses).

2.5.1 Thermodynamics of the Fe-O System

Thermodynamically, oxidation reactions with air or oxygen can be represented by:

$$xM + \frac{y}{2}O_2 \rightarrow M_xO_y \qquad (2.15)$$

where x and y are integers, M metals, and M_xO_y the metal oxides. The change in free energy, ΔG, can be expressed as (Gaskell 1981)

$$\Delta G = \Delta G_{oxide} - \Delta G_{react} \qquad (2.16)$$

$$\Delta G = \Delta G^0(M_xO_y) - \frac{y}{2}RT\ln p_{O2} \qquad (2.17)$$

$$\Delta G = RT\ln p^0_{O_2} - \frac{y}{2}RT\ln p_{O_2} \qquad (2.18)$$

$$\Delta G = \frac{y}{2} RT \ln\left(\frac{p^0_{O_2}}{p_{O_2}}\right) \qquad (2.19)$$

Where $p^0_{O_2}$ is the oxygen pressure at equilibrium and p_{O_2} is the initial oxygen pressure. If the value of p_{O_2} is higher than $p^0_{O_2}$, ΔG becomes negative and subsequently the metal oxide is formed. When ΔG is equal to zero, $p^0_{O_2}$ is called the dissociation oxygen pressure. Since this critical value increases as the temperature increases, oxidation becomes more favorable with increased temperature.

Prediction of which Fe oxide will form under particular conditions is often important for planning laboratory or industrial syntheses. The change in free energy, ΔG can provide information about which compounds are thermodynamically feasible under given conditions. The free energy or chemical potential is the driving force of the reaction and decreases until the system is at equilibrium. If the free energy change is negative, therefore, the products are stable with respect to the reactants.

To calculate the total free energy change of reaction, ΔG, it is necessary to know the standard molar free energy of formation, ΔG^0, of each component involved in the reaction. For a solid, the standard state refers to a pure substance in its most stable form under reference condition of pressure and temperature, 0.1 MPa and 25°C (289.15 K).

Table 2.2 lists the ΔG^0, ΔH^0 and ΔS^0 values for the iron oxides, and Table 2.3 for the soluble Fe species with other compounds or elements involved and needed for calculating the free energy change of reaction involving the formation of iron oxides.

Table 2.2 Standard free energies, enthalpies and entropies of formation of iron oxides at 0.1 MPa and 298 K (Cornell and Schwertmann 2003)

Solid	ΔH_f^0 *kJ mol*$^{-1}$	ΔS_f^0 *kJ mol*$^{-1}$*K*$^{-1}$	ΔG_f^0 *kJ mol*$^{-1}$	*Source*
Goethite	559.3	60.5	488.6	1
			488.8	2
			482.9	3
	562.9	60.38[0]	492.1	4
Lepidocrocite			477.7	5
	554.6			11
	556.4	62.5	486.3	12[&]
Akaganéite			752.7	6
	557.6			11
Ferrihydrite			699	3
			(712)	
$Fe(OH)_2$	569	87.9	486	7
	568.8	79.59	484.2	8
			492	3
Hematite	824.6	87.4	742.7	1
	823.13	90.06	741.8	8
	828.2	87.7	746.2	9
	826.2	87.4	744.3	10, 16
Magnetite	−1115.7	146.1	1012.6	1, 10
	1118.4	146.6	1015.1	8
	1119.5	145.9	1016.1	9
h-Magnetite			945.79	17
Maghemite			711.14	3
Maghemite$_{tetr.}$	812.7			11
	805.8	87.4	723.9	13[&;]
Maghemite$_{cubic}$	−812.3			11
	−805.8	91.4	725.1	13[&;]
FeO	272	59.8	251	1
	−264.0		−243.5	18
Wüstite	266.3	54.03	244.6	8
	272	60.82	251.74	9
Green Rust*-SO_4			−3795 ± 15	14
Ditto			−3669 ± 4	15
Green Rust**-Cl			−2146 ± 5	14
Green Rust*-CO_3			−3590 ± 10	14

1) Robie et al., 1978; 2) Berner, 1969; 3) Langmuir, 1969, 1971; 4) Diakonov et al., 1994; 5) Van Schuylenborgh, 1973; 6) Calc. by Murray, 1979; 7) Wagman et al., 1982; 8) Garrels & Christ, 1965; 9) Helgeson, 1969; 10) Hemingway, 1990, 11) Laberty & Navrotsky, 1998; 12) Diakonov, 1998; 13) Diakonov 1998a; 14) Refait et al., 1999; 15) Hansen et al. 1994; 16) O'Neill, 1988; 17) Stolen & Gronvold, (1996); 18) Haavik et al. (2000)

* $Fe_4^{II}Fe_2^{III}(OH)_{12}SO_4$; ** $Fe_3^{II}Fe^{III}(OH)_8Cl$; + $Fe_4^{II}Fe_2^{III}(OH)_{12}CO_3$; ∮ computed from Lindsay (1979)

0 natural sample; & calculated

Table 2.3 Standard free energies, enthalpies and entropies for soluble Fe and some other species at 298 K (Cornell and Schwertmann 2003)

Species	ΔH^0 *kJ mol*$^{-1}$	ΔS^0 *kJ mol*$^{-1}$*K*$^{-1}$	ΔG^0 *kJ mol*$^{-1}$	*Source*
Fe^{3+}	−49.6	−277	17.2	6
	47.75	293	10.55	2
			−16.83	3
Fe^{2+}	89.1	138	−78.8	2
$FeOH^{2+}$	324	29.2	229.4	2
			−240.2	4
$Fe(OH)_2^+$			−438	2
$Fe_2(OH)_2^{4+}$			467.3	2
$Fe(OH)_2$	−1050	74	−845	5
			−814.6	1
$FeOH^+$			277.3	2
H_2O_1			238.2	2
OH^-	230	10.75	157.5	2
H^+			0	
H_2	0	130.6	0	2
O_2 g	0	205	0	2
O_2 aq.	11.7	111	16.32	2
			27.3	
Fe	0	27.3	0	2

1) Langmuir, 1969; 2) Wagman et al., 1982; 3) Garrels & Christ, 1965; 4) Baes & Messmer, 1976; 5) Diakonov et al. 1999; 6) Shock & Helgeson, 1988.

2.5.2 Stability of Iron Oxide

The lists of Standard free energies, enthalpies and entropies can also be used to calculate the relative stabilities of the different iron oxides. The stability domains of these compounds are commonly plotted as functions of two variables, the most important of which are pH, Eh, temperature and p_{O_2}. A stability diagrams provides a guide to what compound may form under any particular conditions.

Stability diagrams frequently involve the hematite/magnetite pair. The variables used depend upon whether the oxidation of magnetite to hematite is written in terms of O_2 or H_2O. However, the data plotted in stability diagram may not be in accord with that actually observed. The reasons for this are: first, meta-stable phases

can exist for long periods of time and second, the thermodynamic data available may not apply to the existing phases. Also the stability of the oxide may depend on particle size and therefore surface energy must be taken into account. Figures 2.11- 2.13 show the stability domain for iron and iron oxide as a function of temperature and oxygen content (Fe-O phase diagrams). The phase diagrams are for the system at equilibrium; therefore, a phase observed at a high temperature may be different than that predicted by the equilibrium phase diagram because equilibrium has not been achieved.

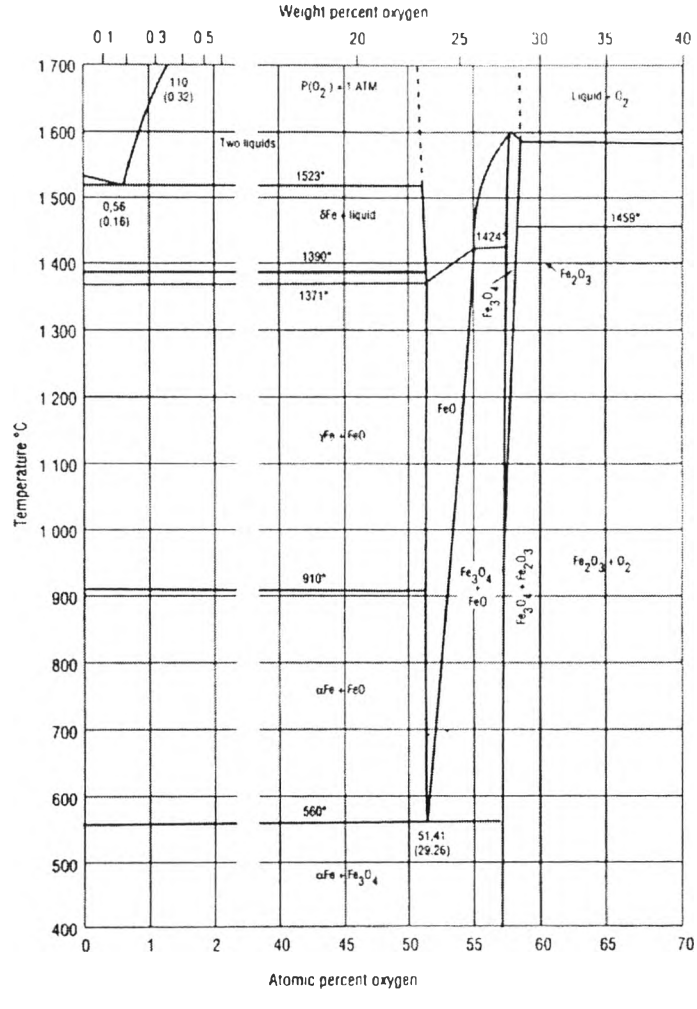

Figure 2.11 Equilibrium phase diagram for the iron-oxygen system (Hansen, Anderko et al. 1965).

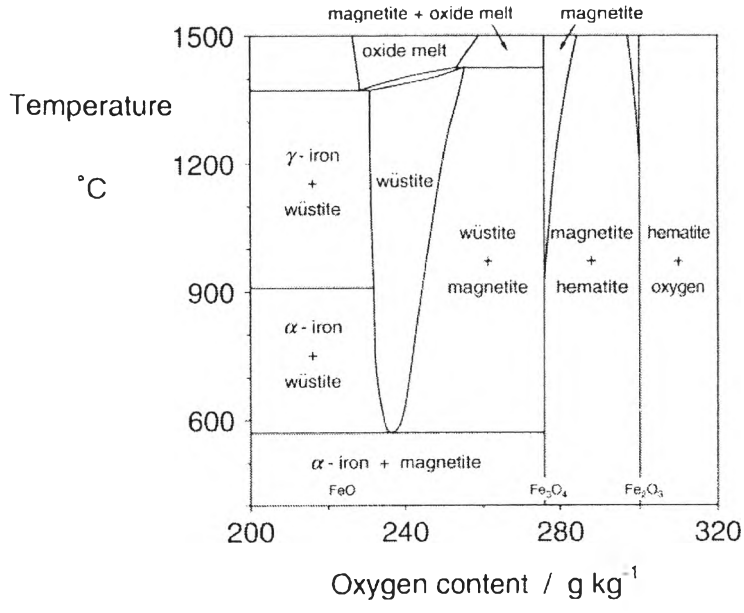

Figure 2.12 Phase diagram of the Fe-O system (Bogbandy & Engell, 1971, referenced in The Iron Oxides: Structure, Properties, Reactions, Occurences and Uses).

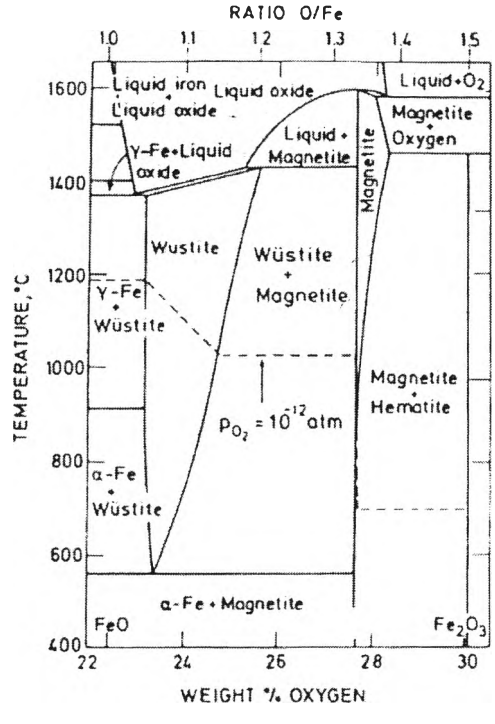

Figure 2.13 The iron-oxygen phase diagram (Kofstad 1988).

The Ellingham/Richardson diagram explains the variation of the standard free energy for the formation of the oxides as a function of temperature. The case of iron oxidation is shown in Figure 2.14 (Gaskell 1981). For oxidation above 570°C, wustite is more stable than magnetite. This means that wustite will likely decompose into iron and magnetite below 570°C.

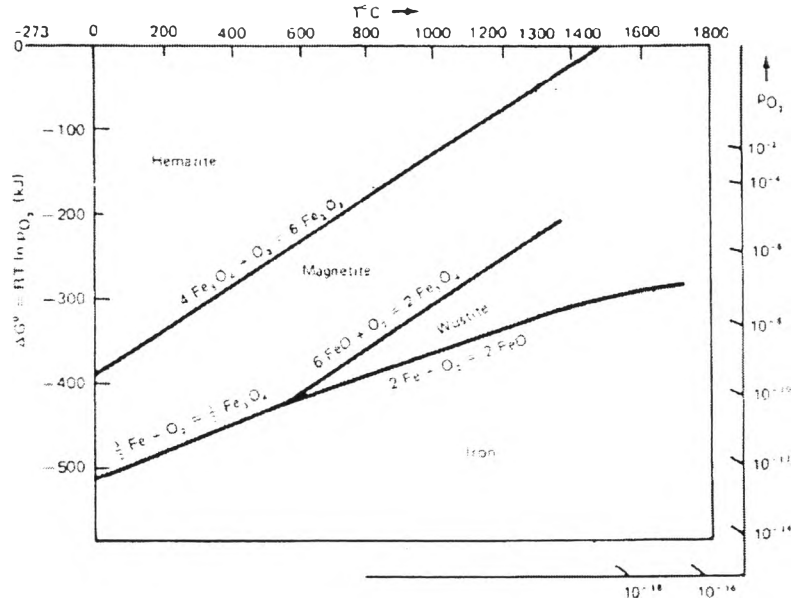

Figure 2.14 The Ellingham/Richardson diagram for iron oxides (Gaskell 1981).

2.5.3 Oxidation Mechanism of Iron

The mechanism of iron oxidation can divided into two stages; 1) initial oxidation, initially proceeding at a linear rate, followed by a parabolic rate of oxidation, and 2) diffusion-controlled oxidation by ionic species through the newly formed oxide layer (Davies, Simnad et al. 1951; Abuluwefa, Guthrie et al. 1996).

The initial stage of iron oxidation can be divided into four reactions as illustrated in Figure 2.15: a) chemisorption of oxygen, b) formation of a fine mosaic layer, c) growth of the oxide crystal, and d) appearance of the second layer (Gulbransen and Ruka 1952). In oxidation below 570°C, the overall oxidation rate is controlled by the growth rate of Fe_3O_4. At intermediate temperatures between 350 and 500°C, Fe_3O_4 nucleates and grows laterally over the surface. Once the thin layer

is completely covered, the growth rate of Fe_3O_4 is parabolic. Due to the lower effective p_{O_2} at the Fe_3O_4 surface, the growth rate of Fe_3O_4 is slow, and nucleation and lateral growth by Fe_2O_3 occurs.

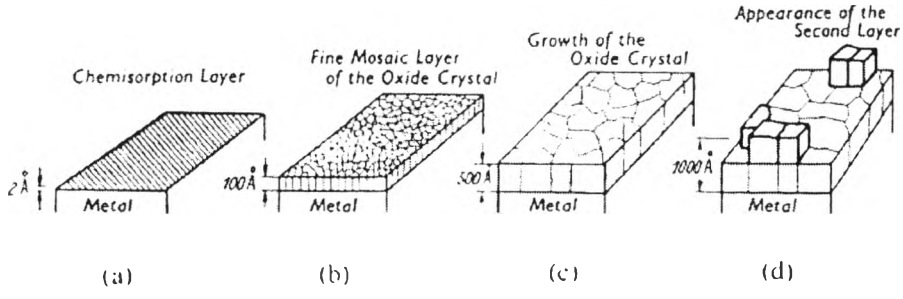

Figure 2.15 Schematic representation of oxide layer growth on iron: (a) chemisorption of oxygen; (b) the formation of a fine mosaic layer; (c) growth of the oxide crystal; (d) appearance of the second layer (Gulbransen and Ruka 1952).

2.5.4 Formation and Transformation of Iron Oxide

In essence, formation of an oxide involves two basic mechanisms: direct precipitation from Fe(II)- or Fe(III)- containing solution and transformation of Fe oxide precursor, either by a dissolution/reprecipitation process or via a solid state transformation involving internal rearrangements within the structure of the solid precursor. The transformations have an important role in corrosion processes and in processes occurring in various natural environments. Transformations without chemical changes are termed isochemical. Transformations that involve chemical modification are dehydration (loss of H_2O), dehydroxidation (loss of OH) and oxidation/reduction (a turnover of electrons). Structurally, the transformation processes are either topotactic or reconstructive. A topotactic transformation takes place within the solid phase. It involves internal atomic rearrangements with a single crystal of the initial phase being transformed into a single crystal of another phase. The reconstructive transformation involves dissolution/reprecipitation which the initial phase

breakdown (dissolve) completely and the new phase precipitates from solution, therefore, no structural relationship between the precursor and product.

Table 2.4 Interconversions among the iron oxides (Cornell and Schwertmann 2003)

Precursor	*Product*	*Type of transformation*	*Preferred medium*
Goethite	Hematite	Thermal or mechanical dehydroxylation Hydrothermal dehydroxylation	Gas/vacuum Solution
	Maghemite	Thermal dehydroxylation	Air + organic
Lepidocrocite	Maghemite, Hematite	Thermal dehydroxylation	Gas/vacuum
	Goethite	Dissolution/reprecipitation	Alkaline solution
	Magnetite	Reduction	Alkaline solution with Fe^{II}
Akaganéite	Hematite	Thermal dehydroxylation	Gas/vacuum
	Goethite,	Dissolution/reprecipitation	Alkaline solution
	Hematite	Dissolution/reprecipitation	Acid solution
	Magnetite	Dissolution/reduction	Alkaline solution with N_2H_4
δ-FeOOH	Hematite	Thermal dehydroxylation	Gas/vacuum
Feroxyhyte	Goethite	Dissolution/reprecipitation	Alkaline solution
Ferrihydrite	Hematite, Maghemite	Thermal dehydration/dehydroxylation	Gas/vacuum
	Goethite,	Dissolution/reprecipitation	Aqueous solution pH 3–14,
	Akaganéite,	" "	Acidic media; presence of Cl
	Lepidocrocite	" "	pH 6, presence of cysteine
	Hematite,	Aggregation, short-range crystallization within ferrihydrite aggregate	Aqueous solution at pH 6–8
	Substituted magnetite	Dissolution/reprecipitation	Alkaline solution with M^{II}
Hematite	Magnetite	Reduction	Reducing gas
		Reduction-dissolution reprecipitation	Alkaline solution with N_2H_4
Magnetite	Maghemite, Hematite	Oxidation	Air
Maghemite	Hematite	Thermal conversion	Air
$Fe(OH)_2$	Magnetite	Oxidation	N_2; Alkaline solution
	Goethite,		Alkaline solution
	Lepidocrocite,		
	Magnetite,		
	Maghemite		
FeO	Magnetite (+Fe)	Disproportionation	Air

2.5.5 Oxidation of Magnetite to Maghemite or Hematite

In the dry state, magnetite is readily oxidized to maghemite by air. Magnetite can change (over years) from black to the brown of maghemite at room temperature. At temperatures over 300°C, the transformation proceeds further to hematite.

Oxidation of magnetite under these conditions involves a topotactic reaction in which the original crystal morphology is maintained throughout. During the reaction, the density of the starting material falls and the weight of the sample increases because oxygen is taken up:

$$4Fe_3O_4 + O_2 \rightarrow 6Fe_2O_3 \qquad (2.21)$$

However, no porosity develops and the sample surface area does not change.

Oxidation to maghemite involves a reduction in the number of Fe atoms per unit cell of 32 oxygen ions, from 24 in magnetite to 21⅓ in magnetite. The reaction proceeds by outward migration of the cations toward the surface of the crystal together with the creation of cation vacancy and the addition of oxygen atoms. At the surface the cations are oxidized and interact with adsorbed oxygen to form a rim of maghemite.

2.5.6 Kinetics of High Temperature Oxidation/Corrosion of Iron in Gases

Iron reacts chemically with oxygen in air to form a surface film of oxide at temperatures ranging from below room temperature to temperatures of up to 1000°C. The films formed at room temperature are only a few Å thick and hence are invisible, but at higher temperatures, thick scales are produced. This type of corrosion involves an oxidation/reduction reaction and occurs in the dry state. The reaction takes place in the oxide layer and the limiting factor is the availability of oxygen.

The formation of an oxide layer is thermodynamically favorable and kinetically rapid at room temperature, but as the temperature rises, the free energy of oxide formation (originally negative) increases to the point where the metal, oxide and oxygen are in equilibrium. At temperatures above this equilibrium, and if the oxygen partial pressure is low enough, the oxide can decompose.

On a freshly cleaned iron surface, oxidation is initially fast, but as the oxide layer grows, it acts as a barrier between the interacting species and the reaction

rate soon falls. The higher the temperature, the thicker the film before the reduction in oxidation rate becomes significant.

At high temperatures the oxidation rate k is initially, rectilinear,

$$x = kt + m, \qquad (2.22)$$

where x is the thickness of the film, t is the time, and m is a constant.

With time and increasing film thickness and coherency, the kinetics change and the reaction is now controlled by outward diffusion of metal ions and electrons across the film, together with possible migration of anions inwards (as show in Figure 2.16) A parabolic (Wagner's) law is now obeyed.

$$x^2 = kt + m \qquad (2.23)$$

This parabolic law, which indicates that diffusion is rate-limiting, is of overwhelming importance for scale formation. Wagner,1933 (referenced in *The Iron Oxides: Structure, Properties, Reactions, Occurences and Uses*) showed that the parabolic scale constant can be calculated using the enthalpy of formation of the corrosion product, the electrical conductivity of the protective film and the transport number of the ions and electrons in the film.

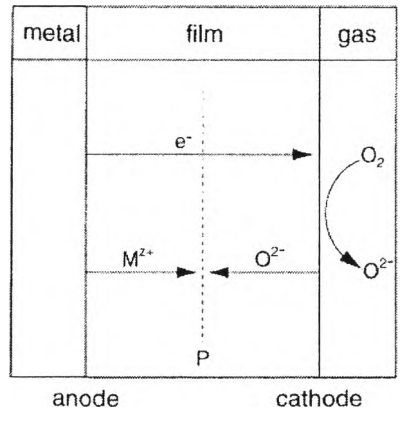

Figure 2.16 Schematic representation of oxidation of iron. P = plane of growth (West, 1980, referenced in The Iron Oxides: Structure, Properties, Reactions, Occurences and Uses).

The parabolic law is obeyed only over the temperature range over which a continuous oxide layer forms. Whether or not the oxide layer is coherent depends upon the ratio of the volume of oxide formed to the volume of iron corroded to produce the film. For iron, the ratio is 2.1 which indicates that the oxide occupies a larger volume than does the amount of iron consumed. Therefore, the film is under compression and as it thickens (> 10 nm), stresses and flaws develop. When this happens the parabolic law no longer operates and growth may be either quasi linear or logarithmic. The different types of possible kinetic plots are shown in Figure 2.17.

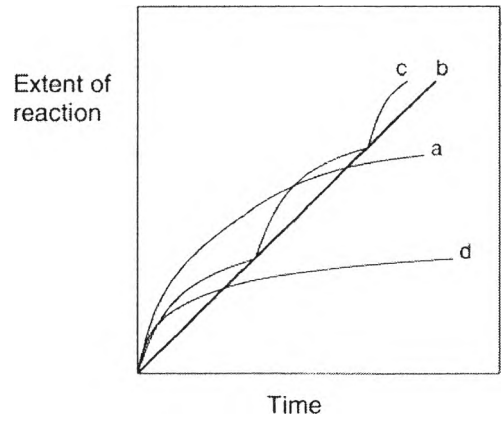

Figure 2.17 Plots of the growth laws of oxidation: a) parabolic, b) rectilinear, c) quasi-rectilinear, d) logarithmic (West, 1980, referenced in The Iron Oxides: Structure, Properties, Reactions, Occurences and Uses).

Low temperature (< 400°C) oxidations of iron follow a logarithmic law,

$$x = ln\ (kt) \qquad (2.24)$$

The oxidation rate which follows this law is thought to be due to reduced electronic conductivity as the film thickens, rather than to cracks in the film.

2.5.7 Effect of Alloying Elements on Oxidation Rates

The effect of alloy additions on oxidation will depend on the behavior of the particular element added with respect to oxidation. If the added element has less affinity for oxygen than iron, it will tend to concentrate at the surface and might alter the kinetics of the overall oxidation of the alloy. On the other hand, if the added element has a higher affinity for oxygen than iron, it will be oxidized preferentially and form an oxide product which will alter the oxidation kinetics. An example of this is chromium in steel which oxidizes preferentially and forms an adherent, compact chromium oxide layer at the metal surface, considerably slowing down the kinetics of oxidation due to the slower rate of diffusion of cations and anions through chromium oxides relative to iron oxides.

2.5.7.1 Effect of Carbon

Carbon is added to steel to improve its physical properties. When carbon is present in the steel, during oxidation, it will tend to diffuse to the reaction surface and react with oxygen to form carbon monoxide or carbon dioxide. The formed carbon monoxide at the reaction surface can alter the oxidation rates mainly in two ways: first, it will play a role in determining the equilibrium oxygen potential at the reaction surface, due to the added carbon-oxygen reaction at the interface. Second, if the formed carbon monoxide or carbon dioxide cannot escape from the reaction surface, it would have the tendency to retard oxidation as a result produce pore formation at the metal/oxide interface (Abuluwefa 1996).